

Dependence of limited radiative recombination rate of InGaN-based light-emitting diode on lattice temperature with high injection

Jiang-Dong Gao(高江东), Jian-Li Zhang(张建立), Zhi-Jue Quan(全知觉), Jun-Lin Liu(刘军林), Feng-Yi Jiang(江风益)

Citation: Chin. Phys. B . 2020, 29(4): 047802 . **doi:** 10.1088/1674-1056/ab790a
Journal homepage: http://cpb.iphy.ac.cn; http://iopscience.iop.org/cpb

What follows is a list of articles you may be interested in

Optoelectronic properties analysis of silicon light-emitting diode monolithically integrated in standard CMOS IC

Yanxu Chen(陈彦旭), Dongliang Xu(许栋梁), Kaikai Xu(徐开凯), Ning Zhang(张宁), Siyang Liu(刘斯扬), Jianming Zhao(赵建明), Qian Luo(罗谦), Lukas W. Snyman, Jacobus W. Swart

Chin. Phys. B . 2019, 28(10): 107801 . **doi:** 10.1088/1674-1056/ab3e44

Improvement of electro-optic performances in white organic light emitting diodes with color stability by buffer layer and multiple dopants structure

Zhi-Qi Kou(寇志起), Yu Tang(唐宇), Li-Ping Yang(杨丽萍), Fei-Yu Yang(杨飞宇), Wen-Jun Guo(郭文军)

Chin. Phys. B . 2018, 27(10): 107801 . **doi:** 10.1088/1674-1056/27/10/107801

Characteristic improvements of thin film AlGaInP red light emitting diodes on a metallic substrate

Bin Zhao(赵斌), Wei Hu(胡巍), Xian-Sheng Tang(唐先胜), Wen-Xue Huo(霍雯雪), Li-Li Han(韩丽丽), Ming-Long Zhao(赵明龙), Zi-Guang Ma(马紫光), Wen-Xin Wang(王文新), Hai-Qiang Jia(贾海强), Hong Chen(陈弘)

Chin. Phys. B . 2018, 27(4): 047803 . **doi:** 10.1088/1674-1056/27/4/047803

High color rendering index white organic light-emitting diode using levofloxacin as blue emitter

Miao Yan-Qin, Gao Zhi-Xiang, Zhang Ai-Qin, Li Yuan-Hao, Wang Hua, Jia Hu-Sheng, Liu Xu-Guang, Tsuboi Taiju

Chin. Phys. B . 2015, 24(5): 057802 . **doi:** 10.1088/1674-1056/24/5/057802

Improvement of electron injection of organic light-emitting devices by inserting a thin aluminum layer into cesium carbonate injection layer

Xin Li-Wen, Wu Xiao-Ming, Hua Yu-Lin, Xiao Zhi-Hui, Wang Li, Zhang Xin, Yin Shou-Gen

Chin. Phys. B . 2015, 24(3): 037802 . **doi:** 10.1088/1674-1056/24/3/037802

Dependence of limited radiative recombination rate of InGaN-based light-emitting diode on lattice temperature with high injection*

Jiang-Dong Gao(高江东), Jian-Li Zhang(张建立)†, Zhi-Jue Quan(全知觉), Jun-Lin Liu(刘军林), and Feng-Yi Jiang(江风益)

National Institute of LED on Silicon Substrate, Nanchang University, Nanchang 330096, *China*

(Received 16 January 2020; revised manuscript received 18 February 2020; accepted manuscript online 24 February 2020)

It is observed that the radiative recombination rate in InGaN-based light-emitting diode decreases with lattice temperature increasing. The effect of lattice temperature on the radiative recombination rate tends to be stable at high injection. Thus, there should be an upper limit for the radiative recombination rate in the quantum well with the carrier concentration increasing, even under the same lattice temperature. A modified and easily used ABC-model is proposed. It describes that the slope of the radiative recombination rate gradually decreases to zero, and further reaches a negative value in a small range of lattice temperature increasing. These provide a new insight into understanding the dependence of the radiative recombination rate on lattice temperature and carrier concentration in InGaN-based light-emitting diode.

Keywords: InGaN-based light-emitting diode, carrier recombination, ABC-model, lattice temperature

PACS: 78.60.Fi, 85.30.–z, 81.05.Ea **DOI:** 10.1088/1674-1056/ab790a

1. Introduction

InGaN-based light-emitting diodes (LEDs) play an important role in visible lighting applications and have a very broad potential. However, InGaN-based LEDs exhibit that its emitting efficiency decreases significantly with current increasing when operating at high injections. In order to void the low luminous efficiency at high current densities, a large area of InGaN-based LED is required at a low operated current density in order to keep the same luminous flux demand. This leads the illumination cost to increase. In order to reduce cost and make full use of device feature, it is necessary to understand the carrier recombination mechanism. However, the mechanism for reducing the light efficiency of InGaN-based LEDs has become a complicated issue for a long time.

In general, the main carrier recombination processes include the Shockley–Read–Hall (SRH) nonradiative recombination, trap-assisted Auger recombination, intrinsic Auger recombination, and bimolecular radiative recombination. Therefore, radiative internal quantum efficiency (IQE) and recombination current are, respectively, expressed as

$$\eta_i = \int R_{\mathrm{RAD}}\,\mathrm{d}V \Big/ \int \left(R_{\mathrm{SRH}} + R_{\mathrm{TAA}} + R_{\mathrm{AUG}} + R_{\mathrm{RAD}}\right)\mathrm{d}V, \quad (1)$$

$$I = q\int \left(R_{\mathrm{SRH}} + R_{\mathrm{TAA}} + R_{\mathrm{AUG}} + R_{\mathrm{RAD}}\right)\mathrm{d}V, \quad (2)$$

where q is the elementary charge, V is the volume of LED, R_{SRH}, R_{TAA}, R_{AUG}, and R_{RAD} are the SRH nonradiative recombination rate, the trap-assisted Auger recombination rate, the intrinsic Auger recombination rate, and the bimolecular radiative recombination rate, respectively. The SRH nonradiative recombination rate[1,2] and the trap-assisted Auger recombination rate[3,4] are given by

$$\begin{aligned} &R_{\mathrm{SRH}} + R_{\mathrm{TAA}} \\ &= \left(np - n_i^2\right)\left\{\tau_{\mathrm{p}}\left(n + n_1\right)/\left[1 + k_{\mathrm{p}}\left(n + p\right)\tau_{\mathrm{p}}\right]\right. \\ &\quad \left. + \tau_{\mathrm{n}}\left(p + p_1\right)/\left[1 + k_{\mathrm{n}}\left(n + p\right)\tau_{\mathrm{n}}\right]\right\}^{-1}, \end{aligned} \quad (3)$$

where n and p are the electron and hole concentrations, n_i is the intrinsic carrier concentration, τ_{n} and τ_{p} are the electron and hole carrier lifetimes, n_1 and p_1 are the electron and hole concentrations when the quasi-Fermi energy is equal to the trap energy, and k_{n} and k_{p} are the trap-assisted Auger recombination coefficients for electrons and holes, respectively. The intrinsic Auger recombination rate[5–7] is expressed as

$$R_{\mathrm{AUG}} = \left(C_{\mathrm{n}}n + C_{\mathrm{p}}p\right)\left(np - n_i^2\right), \quad (4)$$

where C_{n} and C_{p} are the intrinsic Auger recombination coefficients for electrons and holes, respectively. The bimolecular radiative recombination rate reads

$$R_{\mathrm{RAD}} = B\left(np - n_i^2\right), \quad (5)$$

where B is the bimolecular radiative recombination coefficient. When the carrier recombination mainly occurs in the multi-quantum wells (MQWs), one can obtain the following simple equations with $n = p$ and ignoring n_i^2, the famous ABC-model:

$$\eta_i = Bn/\left(A + Bn + Cn^2 + kAn^2\right), \quad (6)$$

$$I = qV_{\mathrm{E}}\left(An + Bn^2 + Cn^3 + kAn^3\right), \quad (7)$$

*Project supported by the National Natural Science Foundation of China (Grant Nos. 51602141, 11674147, 61604066, 11604137, and 21405076), the National Key Research and Development Project of China (Grant Nos. 2016YFB0400600 and 2016YFB0400601), and the Key Research and Development Project of Jiangxi Province, China (Grant No. 20171BBE50052).

†Corresponding author. E-mail: zhangjianli@ncu.edu.cn

© 2020 Chinese Physical Society and IOP Publishing Ltd

where A, B, C, k, and $V_{\rm E}$ are the coefficients for the SRH nonradiative recombination, the bimolecular radiative recombination, the intrinsic Auger recombination, the trap-assisted Auger recombination, and the effective recombination volume of MQWs, respectively. Therefore, the total radiative recombination rate per unit area of a planar LED can be expressed as follows:

$$R = Bn^2 V_{\rm E}/S_{\rm E}, \tag{8}$$

where $S_{\rm E}$ is the effective injected area which can also be regarded as the effective light emission area of the LED. In the actual experiment testing, the IQE and the total radiative recombination rate per unit area are obtained, respectively, as follows:

$$\eta_i = q\lambda_{\rm ave} P/\eta_{\rm e} hcI, \tag{9}$$

$$R = \lambda_{\rm ave} P/\eta_{\rm e} hcS_{\rm E}, \tag{10}$$

where $\eta_{\rm e}$ is the light extraction efficiency, $\lambda_{\rm ave}$ is the average wavelength, P is the light outputting power, h is the Planck constant, and c is the light speed. Since the light extraction efficiency cannot be directly obtained, it is usually taken to be the maximum external quantum efficiency at low lattice temperatures.[8,9] Thus, by using the ABC-model, physics and experiment are linked to each other through the efficiency and radiative recombination rate.

However, the reality is that this common ABC-model is often difficult to match with experiments at high current densities. This is attributed to the real IQE-droop in InGaN-based LED, which, at high injection, is more serious than that in the modelled LED. The IQE-droop can be understood from two main respects: the increased proportion of the Auger recombination rate[10–12] and the increased proportion of the carrier overflow.[13–15] Since the carrier overflow is usually accompanied with an emission whose wavelength is shorter than that of MQWs,[13,14,16–18] it can be considered that the IQE-droop is due mainly to the Auger recombination when the short wavelength emission is not observed. The increased proportion of the Auger recombination rate is usually due to the reduced effective recombination volume decreasing[19,20] and the radiative recombination coefficient declining.[21–23]

In real InGaN-based thin-film LEDs, the effective recombination volume is mainly limited by the effective light emission area and the number of dominant lighting QWs. Generally, for a good-quality InGaN-based LED, the effective light emission area is quite stable at high current densities. Therefore, the change in the number of effective active QWs will lead to a cliff-like decrease in radiative recombination rate. Thus, it is doubtful that the main cause of the IQE-droop at high injections is the decreasing of effective recombination volume. And then, some scholars believe that the main reason for IQE-droop is the phase-space filling effect[12,22] or the Coulomb-enhanced scattering,[21,24] which reduces the probability of radiative recombination (*i.e.*, the radiative recombination coefficient). The mathematical model of the radiative recombination coefficient is still in controversy. Many researchers[21,22,25,26] believed that the radiative recombination coefficient as a function of carrier concentration should be written as

$$B = B_0/\left[1 + (n/N_*)^x\right], \tag{11}$$

where B_0 is the radiative recombination coefficient in the limit of low carrier concentration, N_* is the effective density of state in QW, and x is a fitting parameter about 1. Due to the existence of the upper limit of the radiative recombination rate at very high current densities,[27–29] the model above can only fit the experimental results at the current densities, which are not very high. Furthermore, due to the increase in lattice temperature, the enhanced extent of imbalance between the increase of carriers in $\boldsymbol{k}$ space and the decrease in carrier mobility will cause the radiative recombination coefficient to decrease. Considering the lattice temperature factor, Shim *et al.*[23] gave the model of the radiative recombination coefficient as follows:

$$B = B_0 \Phi(T,n)/(1 + n/N_*)^y, \tag{12}$$

where Φ is a function relating to the wavevector space, T is the lattice temperature, and y is a fitting parameter between 1 and 2. This model combines the two main factors of carrier concentration and lattice temperature to correct the radiative recombination coefficient. However, the model is complicated and not easy to use.

If only the influence of carrier concentration on radiative recombination is considered as the effect of the coefficient, one result is that the fitting parameter is difficult to confirm directly in experiment. The other result is that some experimental phenomena are neglected. The radiative recombination coefficient describes the radiative recombination rate at the given carrier concentration. Therefore, our interest focuses on the behavior of the radiative recombination rate under the carrier concentration and lattice temperature at high injections to investigate the luminescence mechanism in InGaN-based LEDs. And for simplicity, we will not discuss the phase-space filling effect in Auger recombination here.

2. Experiment and method

The experimental epi-structure growth on 1.2 mm $\times$1.2 mm patterned 2-inch (1 inch = 2.54 cm) Si(111) substrate was performed in a Thomas Swan closed-coupled showerhead metal–organic chemical vapor deposition reactor. Ammonia, trimethylgallium, triethylgallium, trimethylindium, and trimethylaluminum were used as precursors, hydrogen and nitrogen were used as carrier gas. The method of fabricating

InGaN-based LEDs on a Si(111) substrate has been detailed in Refs. [30] and [31]. As shown in Fig. 1, under the 2-μm-thick n-GaN(0001) layer, the 32 periods of InGaN/GaN superlattices (SLs) served as a pre-layer which was composed of periods of alternating 5-nm $In_xGa_{1-x}N$ wells with $x \sim 0.06$ and 1-nm GaN barriers, five green MQWs which were composed of periods of alternating 2.8-nm $In_xGa_{1-x}N$ wells with $x \sim 0.22$ and 12-nm GaN barriers, a 15-nm-thick p-$Al_xGa_{1-x}N$ with $x \sim 0.2$, and a 150-nm-thick p-GaN. The test system contained a temperature controlling unit (K2000, MMR Technologies, Inc., United States), a spectrometer (CAS140CT, Instrument Systems, Germany) equipped with an integrating sphere (ISP250-211, Instrument Systems, Germany), and a direct current (DC) power supply (Keithley 2635, Keithley, United States). Since the lattice temperature is difficult to measure accurately, the pulse current mode was used to drive the LED so that the environment temperature can approach to the lattice temperature. To simplify this problem, we consider the environment temperature here as the lattice temperature.

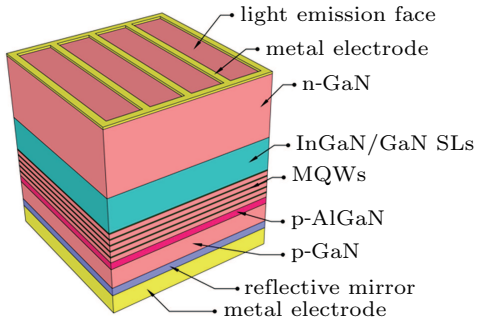


Fig. 1. The schematic diagram of InGaN-based green light-emitting diode grown on Si(111) substrate by metal–organic chemical vapor deposition. As electrode can absorb a large amount of visible light emitted from active region, reflective mirror is often placed between p-GaN and electrode to enhance light extraction efficiency.

3. Results and discussion

Figures 2(a)–2(e) display the electroluminescence spectra of the InGaN-based green LED under 100 K, 150 K, 250 K, 300 K, and 350 K, respectively. It is observed that each spectrum contains only one emission peak whose wavelength ranges from 530 nm to 570 nm. Therefore, within this test range, the overflow of carriers from the MQWs can be ignored.

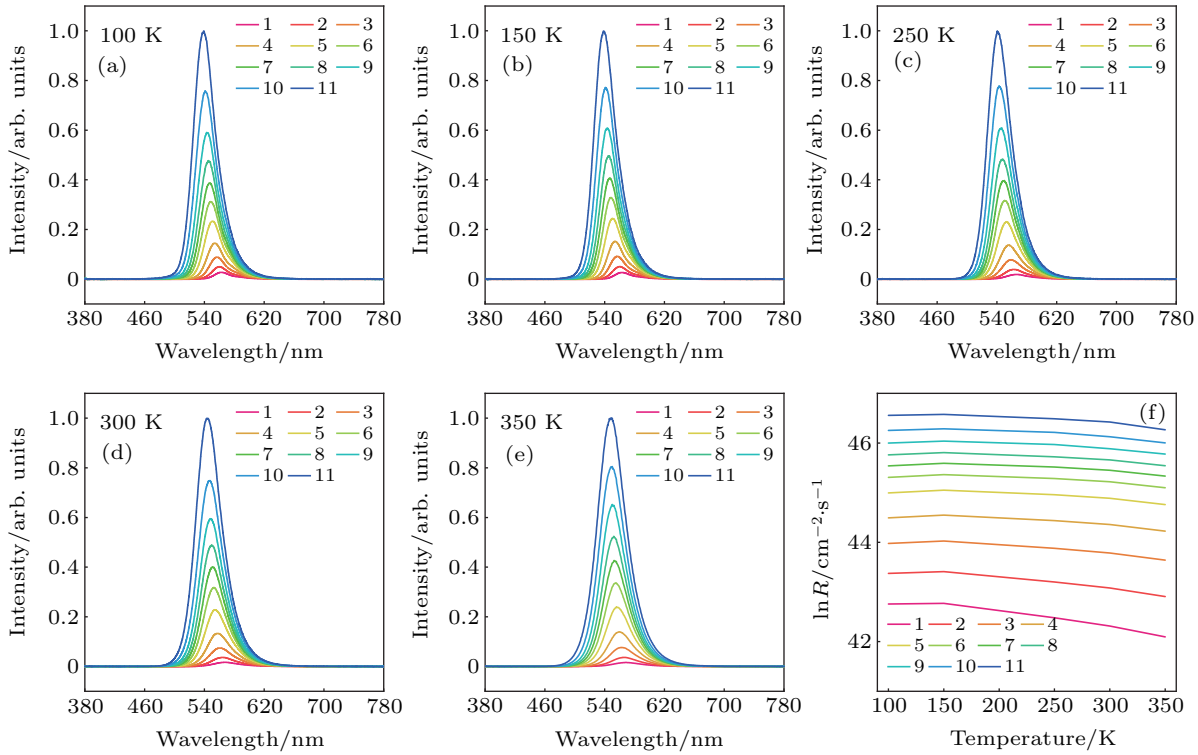


Fig. 2. Experimental electroluminescence spectra of InGaN-based light-emitting diode with different current densities at different lattice temperatures: (a) 100 K, (b) 150 K, (c) 250 K, (d) 300 K, and (e) 350 K, and (f) dependence of the experimental radiative recombination rate R on lattice temperature at different current densities, where lines 1–11 correspond to current density of 0.8 A·cm^{-2}, 1.5 A·cm^{-2}, 3.1 A·cm^{-2}, 5.7 A·cm^{-2}, 10.3 A·cm^{-2}, 15.4 A·cm^{-2}, 20.6 A·cm^{-2}, 26.7 A·cm^{-2}, 36.0 A·cm^{-2}, 51.4 A·cm^{-2}, and 77.1 A·cm^{-2}, respectively.

According to Eq. (10), the total radiative recombination rates per unit area can be obtained at different current densities and lattice temperatures. Figure 2(f) displays the total radiative recombination rates per unit area at different lattice temperatures and current densities. Due to the increase in lattice temperature, the increased SRH non-radiative recombination coefficient would lead to a reduced carrier concentration, under the same current density. However, it is found that the gradient of natural logarithm of the total radiative recombination rate per unit area at lattice temperature approaches to a con-

stant as current density increases. This means that the gradient is almost linear, independent of the carrier concentration and close to $\partial \ln R/\partial T$ at high injections. It is worth noting that the effective recombination volume is determined by the effective recombination length of QW, the number of effective active QWs, and the in-plane distribution of current. First, the effective recombination length of QW increases with current density increasing due to the charge screen of quantum-confined Stark effect,[32] and then turns close to the thickness of QW at high current density. Second, the number of effective active QWs decreases with current density increasing due to the unbalance between electron and hole transport, and then the QWs accumulate near p-side at high current density.[33,34] Third, the in-plane distribution of current fluctuations at low current density tends to be stable at high current density. Therefore, the large fluctuations in gradient at low current densities is main attributed to the fluctuations in effective recombination volume with lattice temperature at low current densities, and the effective recombination volume can be considered to be close to the volume of QW at high current densities. Thus, at high injections, the fluctuation in gradient can be given as follows:

$$BV_{\mathrm{E}}/S_{\mathrm{E}} \propto \exp(\mu T), \tag{13}$$

and after normalization, we have

$$B \propto \exp(-\omega T), \tag{14}$$

where μ and ω are the constants for fitting.

It should be noted that the radiative recombination rate does not increase forever, which is a common sense. The specific behavior is that the radiative recombination rate will reach a maximum value with the current density increasing when the current density is extremely high.[27–29] This seems to be attributed only to the decrease in the radiative recombination coefficient, caused by increasing the lattice temperature when heat dissipation is poor. However, for Eq. (11), the radiative recombination rate is allowed to increase quickly with carrier concentration rising. The lattice temperature of the MQWs needs increasing rapidly to a very high level (more than 1000 K) as the current density increases to satisfy the upper limit of the radiative recombination rate. It is hard to believe that the materials can withstand such a high lattice temperature. Therefore, with the carrier concentration increasing, the radiative recombination rate will reach a constant, even the lattice temperature need not increase. It can explain that the slope of the radiative recombination rate will gradually decrease to zero, and then show a negative value in a small range of increased lattice temperature. Equation (12) is also consistent with the above discussion, but slightly many parameters need fitting. Since the power y is considered to be related to carrier concentration, it may make the things difficult to quantify. All parameters in Eqs. (11) and (12) should be the basic properties of the material, so the powers should be fixed at 2. Here we use the form of Eq. (11). Therefore, at high injections, the radiative recombination rate should be

$$R_{\mathrm{RAD}} \propto n^2/\left[1+(n/N_*)^2\right]. \tag{15}$$

Combining with Eq. (14), the radiative recombination coefficient at high injections should be expressed as follows:

$$B = B_0 \exp(-\omega T)/\left[1+(n/N_*)^2\right], \tag{16}$$

where B_0 is the radiative recombination coefficient in the limit of low carrier concentration and low lattice temperature. Figure 3 clearly describes the dependence of the radiative recombination rate on carrier concentration and lattice temperature. When the carrier concentration is high enough, the suppressed effect from the increase in lattice temperature begins to appear (see the grey area in Fig. 3).

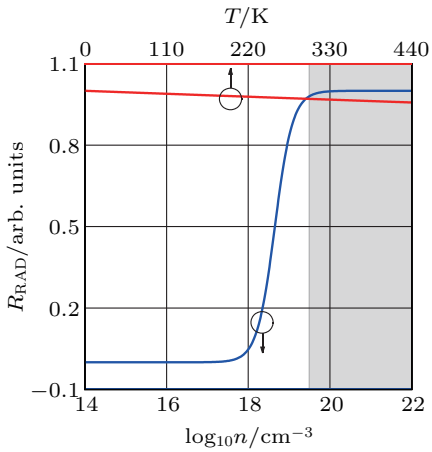


Fig. 3. Dependence of radiative recombination rate on logarithmic carrier concentration (blue line) and lattice temperature (red line), with grey area representing carrier concentration range when radiative recombination rate is mainly influenced by lattice temperature.

The new modified *ABC*-model is used, including Eqs. (6), (7), and (16), to fit the experimental behaviors of IQE and radiative recombination rate at different lattice temperatures and current densities. Hereafter, we use $B_0 = 1.0\times10^{-10}$ cm^3·s^{-1}, $C = 5.5\times10^{-29}$ cm^6·s^{-1}, $k = 1.1\times10^{-36}$ cm^6, $N_* = 4.9\times10^{18}$ cm^{-3}, and $\omega = 1.0\times10^{-4}$, which are all fixed and treated as being linearly independent of lattice temperature, but only treat A as being dependent on lattice temperature (listed in Table 1). All parameters of materials are in the scopes of parameters reported in the literature.[11,12,23,35–38] The effective injected area is 0.97 mm^2, and the effective recombination volume of MQWs at high injection is estimated at 3.11×10^{-9} cm^3, which leads to a close match to the experimental data (see Fig. 4). It can be observed that the new *ABC*-model is well suited for the experimental behaviors under different lattice temperatures and current densities. According to the new model, with the increase of lattice temperature, the decrease of the radiative recombination rate should be divided into two parts: one is the decrease of the carrier concentration, caused by the increase of SRH recombination coefficient

at low current densities and the other is the decrease of radiative recombination coefficient, caused by the increase of lattice temperature at high current densities. Therefore, the best way to improve the luminescence efficiency and radiative recombination rate of InGaN-based LEDs at high current densities is to increase the effective recombination volume, rather than simply to improve the quality of MQWs.

Table 1. Fitted values of A at different lattice temperatures, extracted from modeled results of Fig. 4.

T/K	A/s^{-1}
100	2.0×10^{4}
150	1.6×10^{6}
250	1.4×10^{7}
300	2.1×10^{7}
350	3.5×10^{7}

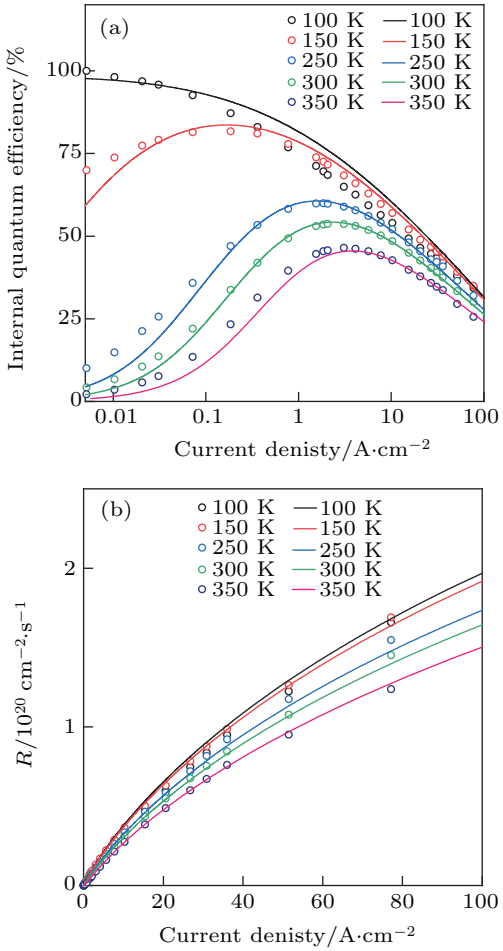


Fig. 4. Comparison between experimental and simulation results by using new *ABC*-model, showing (a) plots of internal quantum efficiency *versus* logarithmic current density and (b) plots of radiative recombination rate versus current density, with circles denoting experiment results, and lines referring to modelled results, for varying values of T and A and fixed values of B_0, C, k, N_*, and ω.

In addition, we believe that the model is also suitable for low injection conditions once the effective recombination volume can be estimated under low injection. Since the effective recombination volume fluctuates easily under small injections, the difference between the model with constant effective recombination volume and the experiment result will be increased.

4. Conclusions

In this work, it is observed that the gradient of logarithm of radiative recombination rate with lattice temperature tends to be stable at high injections. There should be an upper limit of the radiative recombination rate with the increase of carrier concentration in the MQW. Then, a simple modified and easily used *ABC*-model is proposed. It describes that the radiative recombination limited by lattice temperature in InGaN-based LED should be divided into two parts: one is the decrease of the carrier concentration, caused by the increase of SRH recombination at low injection and the other is the decrease of radiative recombination coefficient, caused by the increase of lattice temperature at high injection. These provide a new reference for understanding the radiative recombination mechanism in InGaN-based LEDs.

References

[1] Hall R N 1952 *Phys. Rev.* **87** 387
[2] Shockley W and Read W T 1952 *Phys. Rev.* **87** 835
[3] Fossum J G, Mertens R P, Lee D S and Nijs J F 1983 *Solid-State Electron.* **26** 569
[4] David A, Young N G, Hurni C A and Craven M D 2019 *Phys. Rev. Appl.* **11** 031001
[5] Hangleiter A and Häcker R 1990 *Phys. Rev. Lett.* **65** 215
[6] Kerr M J and Cuevas A 2002 *J. Appl. Phys.* **91** 2473
[7] De Santi C, Meneghini M, La Grassa M, Galler B, Zeisel R, Goano M, Dominici S, Mandurrino M, Bertazzi F, Robidas D, Meneghesso G and Zanoni E 2016 *J. Appl. Phys.* **119** 094501
[8] Laubsch A, Sabathil M, Bergbauer W, Strassburg M, Lugauer H, Peter M, Lutgen S, Linder N, Streubel K, Hader J, Moloney J V, Pasenow B and Koch S W 2009 *Physica Status Solidi C* **6** S913
[9] Shim J I 2017 *III-Nitride Based Light Emitting Diodes and Applications*, Seong T Y *et al.* eds. (Singapore, Berlin, Heidelberg: Springer-Verlag) p. 163
[10] Shen Y C, Mueller G O, Watanabe S, Gardner N F, Munkholm A and Krames M R 2007 *Appl. Phys. Lett.* **91** 141101
[11] Kioupakis E, Rinke P, Delaney K T and Van de Walle C G 2011 *Appl. Phys. Lett.* **98** 161107
[12] Scheibenzuber W G, Schwarz U T, Sulmoni L, Dorsaz J, Carlin J F and Grandjean N 2011 *J. Appl. Phys.* **109** 093106
[13] Shin D S, Han D P, Oh J Y and Shim J I 2012 *Appl. Phys. Lett.* **100** 153506
[14] Shim J I, Kim H, Han D P, Shin D S and Kim K S 2014 *Conference on Gallium Nitride Materials and Devices IX*, February, San Francisco, California, USA, p. 1
[15] Wang L, Meng X, Song J H, Kim T S, Lim S Y, Hao Z B, Luo Y, Sun C Z, Han Y J, Xiong B, Wang J and Li H T 2017 *Chin. Phys. Lett.* **34** 017301
[16] Wu X, Liu J, Quan Z, Xiong C, Zheng C, Zhang J, Mao Q and Jiang F 2014 *Appl. Phys. Lett.* **104** 221101
[17] Lv Q, Liu J, Mo C, Zhang J, Wu X, Wu Q and Jiang F 2019 *ACS Photon.* **6** 130
[18] Zhang Y, Lv Q, Zheng C, Gao J, Zhang J and Liu J 2019 *Superlattices and Microstructures* **136** 106284
[19] Ryu H Y, Shin D S and Shim J I 2012 *Appl. Phys. Lett.* **100** 131109
[20] Ryu H Y, Ryu G H, Choi Y H and Ma B 2017 *Curr. Appl. Phys.* **17** 1298
[21] Smagley V A, Eliseev P G and Osinski M 1997 *Conference on Physics and Simulation of Optoelectronic Devices V*, February, San Jose, California, USA, p. 129
[22] David A and Grundmann M J 2010 *Appl. Phys. Lett.* **96** 103504

[23] Shim J I, Kim H, Shin D S and Yoo H Y 2011 *J. Korean Phys. Soc.* **58** 503
[24] Vallone M, Goano M, Bertazzi F and Ghione G 2017 *J. Appl. Phys.* **121** 123107
[25] Dai Q, Shan Q, Cho J, Schubert E F, Crawford M H, Koleske D D, Kim M H and Park Y 2011 *Appl. Phys. Lett.* **98** 033506
[26] Salis M, Ricci P C and Carbonaro C M 2019 *Appl. Phys. B* **125** 37
[27] Gong Z, Jin S, Chen Y, McKendry J, Massoubre D, Watson I M, Gu E and Dawson M D 2010 *J. Appl. Phys.* **107** 013103
[28] Huang H, Wu H, Huang C, Chen Z, Wang C, Yang Z and Wang H 2018 *Physica Status Solidi (a)* **215** 1800484
[29] Li C C, Zhan J L, Chen Z Z, Jiao F, Chen Y F, Chen Y Y, Nie J X, Kang X N, Li S F, Wang Q, Zhang G Y and Shen B 2019 *Opt. Express* **27** A1146
[30] Jiang F, Zhang J, Sun Q and Quan Z 2019 *Light-Emitting Diodes: Materials, Processes, Devices and Applications*, Li J and Zhang G Q eds. (Cham, Switzerland: Springer International Publishing) pp. 133–170
[31] Jiang F, Zhang J, Xu L, Ding J, Wang G, Wu X, Wang X, Mo C, Quan Z, Guo X, Zheng C, Pan S and Liu J 2019 *Photon. Res.* **7** 144
[32] Usman M, Anwar A R, Munsif M, Malik S and Islam N U 2019 *Superlattices Microstruct.* **135** 106271
[33] David A, Grundmann M J, Kaeding J F, Gardner N F, Mihopoulos T G and Krames M R 2008 *Appl. Phys. Lett.* **92** 053502
[34] Park J H, Kim D Y, Schubert E F, Cho J and Kim J K 2018 *ACS Energy Lett.* **3** 655
[35] Bougrov V, Levinshtein M, Rumyantsev S and Zubrilov A 2001 *Properties of Advanced Semiconductor Materials*: GaN, AIN, InN, BN, SiC, SiGe, Levinshtein M E, *et al.* eds. (New York: John Wiley & Sons) pp. 1–30
[36] Zubrilov A 2001 *Properties of Advanced Semiconductor Materials*: GaN, AIN, InN, BN, SiC, SiGe, Levinshtein M E, *et al.* eds. (New York: John Wiley & Sons) pp. 49–66
[37] Delaney K T, Rinke P and Van de Walle C G 2009 *Appl. Phys. Lett.* **94** 191109
[38] Liu W, Zhao D, Jiang D, Chen P, Liu Z, Zhu J, Li X, Liang F, Liu J, Zhang L, Yang H, Zhang Y and Du G 2016 *J. Phys. D: Appl. Phys.* **49** 145104